Joint Diseases and Related Surgery

Jt Dis Relat Surg
2026;37(1):88-97

ORIGINAL ARTICLE

Effects of Schanz screw location on reduction efficiency in distal femur fractures: A finite element analysis

Shou-I Chen, PhD[1], Wei-Sheng Hong, BS[1], Chia-Che Lee, MD[2], Hung-Kuan Yen, MD[2], Tzu-Hao Tseng, MD, PhD[2*], Shau-Huai Fu, MD, PhD[2,3*]

[1]Department of Mechanical Design Engineering, National Formosa University, Huwei Township, Yunlin County, Taiwan
[2]Department of Orthopaedic Surgery, National Taiwan University Hospital, Taipei City, Taiwan
[3]Department of Orthopedics, National Taiwan University Hospital Yun-Lin Branch, Douliu City, Yunlin County, Taiwan

ABSTRACT

Objectives: The aim of this study was to evaluate the biomechanical efficiency of different Schanz screw positions for indirect reduction of distal femur fractures using finite element analysis.

Materials and methods: A three-dimensional finite element model of a comminuted distal femur fracture was constructed, incorporating relevant anatomical structures including ligaments, menisci, and the gastrocnemius muscle. A 30 N posterior force simulated gastrocnemius-induced deformity, followed by a 15 N horizontal traction force applied through Schanz screws inserted at six positions (hole 1 to 6) on a standard distal femur locking plate. Residual displacement and reduction ratios were measured to assess reduction efficiency.

Results: The model successfully replicated the characteristic posterior displacement (~15 mm) caused by gastrocnemius contraction. Among the six pin positions, hole 6 (most anterior and distal position) achieved the greatest reduction (12.90 mm) with an 86.83% correction ratio, while hole 4 (most posterior and distal position) performed the worst (26.88%). More anterior and distal pin locations provided superior reduction outcomes due to improved mechanical advantage and alignment with the deforming force vector.

Conclusion: Schanz screw placement significantly influences the effectiveness of traction-assisted reduction in distal femur fractures. Hole position 6 yielded the most optimal biomechanical performance and may serve as a practical reference for optimizing intraoperative pin placement, potentially improving surgical efficiency and outcomes.

Keywords: Comminuted, distal femur fracture, gastrocnemius, indirect reduction.

The annual incidence of distal femur fractures is approximately 8.7 per 100,000 individuals and continues to increase due to the rising prevalence of high-energy trauma and age-related fragility fractures.[1] Despite the heterogeneity in injury mechanisms, early surgical intervention still remains the cornerstone of effective management. Timely operative treatment is critical for preserving articular congruity, promoting early mobilization, and enabling assisted weight-bearing.[2,3] Favorable outcomes depend on meticulous restoration of the joint surface, proper alignment, and limb length, typically achieved through adequate fixation constructs that allow for early functional rehabilitation.[3,4]

Received: August 27, 2025
Accepted: September 12, 2025
Published online: November 04, 2025

Correspondence: Tzu-Hao Tseng, MD. Department of Orthopaedic Surgery, National Taiwan University Hospital, Taipei City, Taiwan.

E-mail: b92401004@gmail.com

Correspondence: Shau-Huai Fu, MD. Department of Orthopedics, National Taiwan University Hospital Yun-Lin Branch, Douliu City, Yunlin County, Taiwan.

E-mail: b90401045@gmail.com

Citation: Chen SI, Hong WS, Lee CC, Yen HK, Tseng TH, Fu SH. Effects of Schanz screw location on reduction efficiency in distal femur fractures: A finite element analysis. Jt Dis Relat Surg 2026;37(1):88-97. doi: 10.52312/jdrs.2026.2575.

©2026 All right reserved by the Turkish Joint Diseases Foundation

This is an open access article under the terms of the Creative Commons Attribution-NonCommercial License, which permits use, distribution and reproduction in any medium, provided the original work is properly cited and is not used for commercial purposes (http://creativecommons.org/licenses/by-nc/4.0/).

Various fixation strategies have been described for distal femur fractures, including single lateral plating, retrograde intramedullary nailing, dual plating, and nail-plate constructs.[1,3-7] The choice of fixation method is typically based on the fracture pattern and advances in implant technology.

Among these, lateral locking plates are commonly employed as bridging devices in comminuted supracondylar fractures, often in conjunction with indirect reduction techniques.[8-11] However, management of hyperextension deformity caused by gastrocnemius tension during indirect reduction remains largely empirical. To illustrate, placing a pillow beneath the supracondylar region during traction is a frequently recommended maneuver to counteract this deforming force.[9,12] Despite such strategies, there is a lack of experimental evidence to objectively guide surgeons on the optimal site and direction of traction. As a result, clinical decisions often rely on subjective experience, which may prolong operative time and potentially compromise surgical outcomes through a trial-and-error process.

To address this gap, the present study utilizes finite element analysis (FEA) to investigate the biomechanical efficiency of various traction pin positions in facilitating indirect reduction of distal femur fractures. To enhance clinical relevance, the selected pin locations correspond to commonly used hole positions on a standard distal femur locking plate. To the best of our knowledge, this is the first study to systematically evaluate this surgical technique through computational modeling. We, therefore, aimed to provide objective, actionable insights which may assist surgeons in optimizing reduction maneuvers and improving operative efficiency and outcomes.

MATERIALS AND METHODS

Model construction

A FEA model was constructed to simulate the reduction of comminuted distal femoral fractures using Schanz screw traction. The model comprised the femur, a simplified tibia, key knee ligaments, the menisci, and the gastrocnemius muscle. All anatomical structures were reconstructed using SolidWorks 2016 (Dassault Systèmes SolidWorks Corp., Vélizy-Villacoublay, France) to replicate relevant anatomical relationships and intraoperative conditions (Figure 1). This setup was intended to replicate the surgical scenario of supracondylar fracture reduction using Schanz screw-assisted traction. This study was conducted using a sawbone model for finite element analysis; hence, Ethics Committee approval was not necessary.

The femoral geometry was derived from a composite Sawbones model (Pacific Research Laboratories, Inc., Vashon, WA, USA), which is commonly used in biomechanical studies for its standardized anatomy and material consistency.

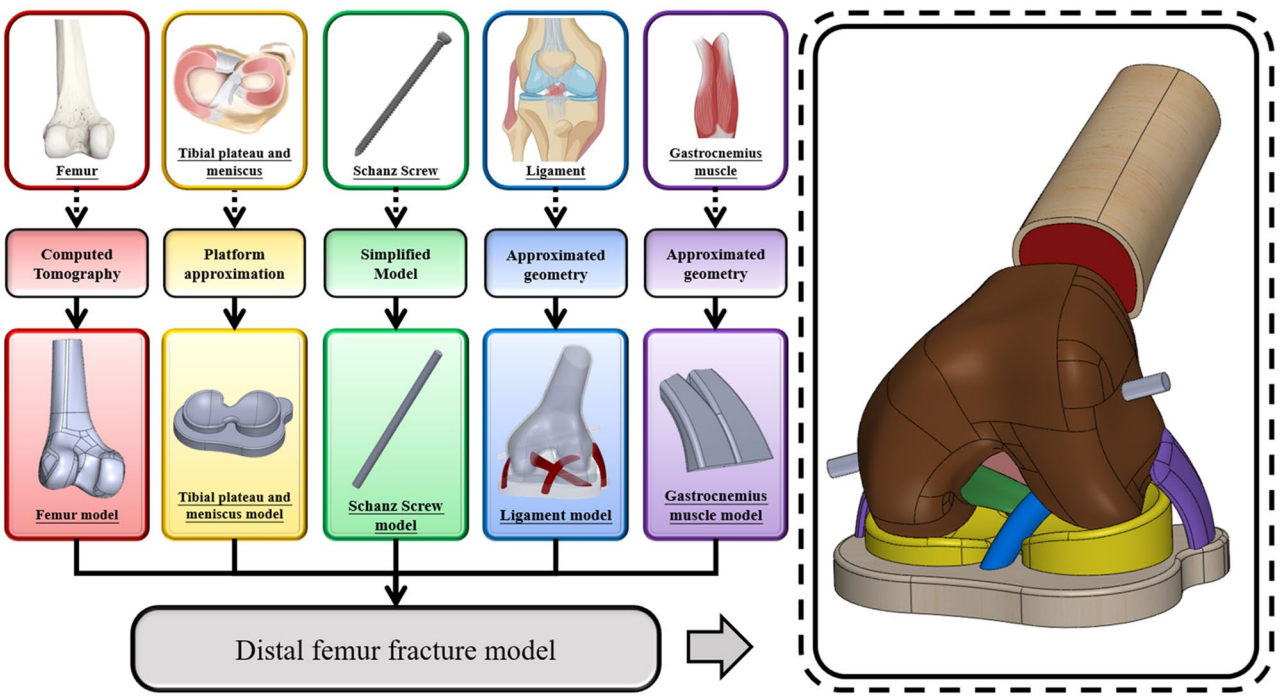


FIGURE 1. Geometric analysis model for reduction of distal femoral comminuted fracture.

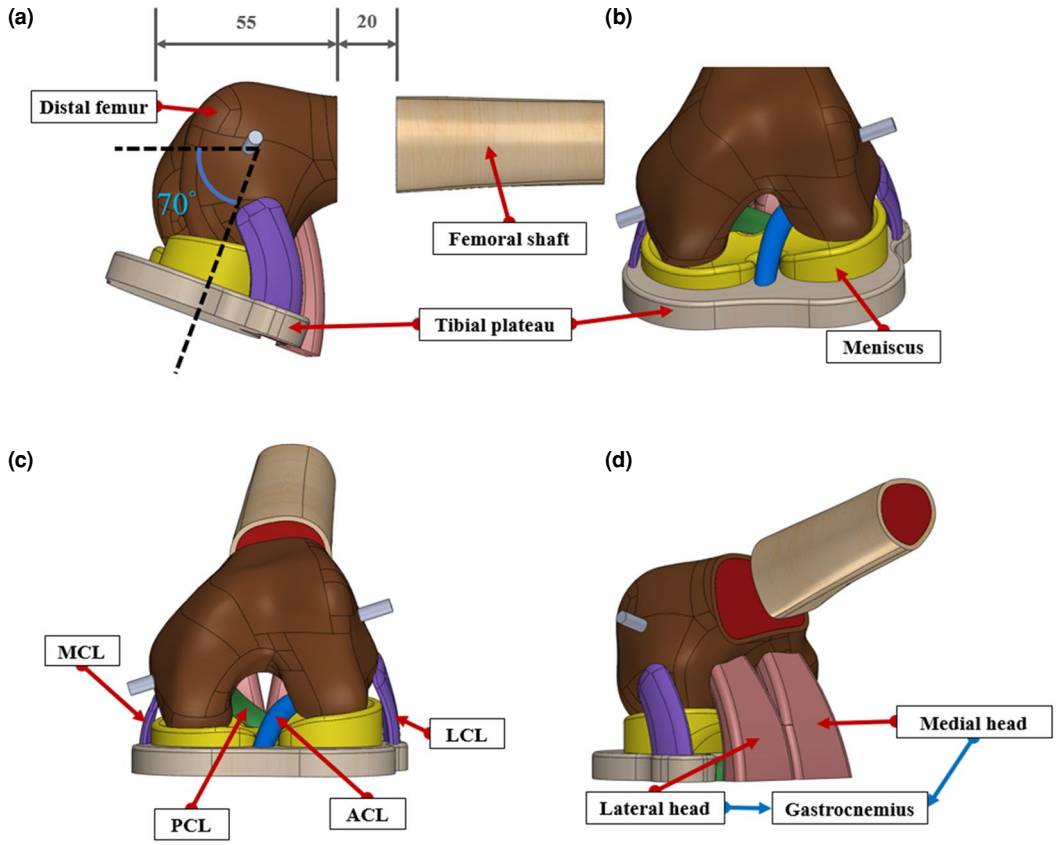


FIGURE 2. Anatomical schematic of the reduction analysis model for the distal femur and surrounding soft tissues.
MCL: Medial collateral ligament; PCL: Posterior cruciate ligament; ACL: Anterior cruciate ligament; LCL: Lateral collateral ligament.

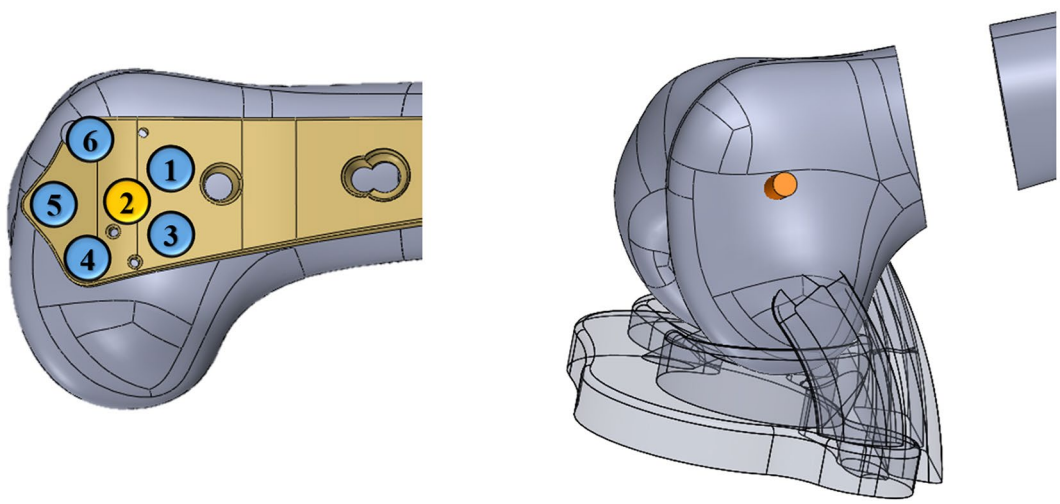


FIGURE 3. Schematic illustration of femoral traction via Schanz screw insertion at various plate hole positions.

The model featured a cortical shell, a cancellous core with a density of 17 pounds per cubic foot (PCF), and a 13-mm intramedullary canal. Computed tomography (CT) scans with 1-mm slice thickness were used to reconstruct a three-dimensional femoral model. To simulate a comminuted fracture, a 20-mm fracture gap was created 55 mm proximal to the distal articular surface (Figure 2a).

The tibia and fibula were simplified as a fixed circular platform to serve as the attachment site for knee ligaments. The anterior cruciate ligament (ACL), posterior cruciate ligament (PCL), medial collateral ligament (MCL), and lateral collateral ligament (LCL) were reconstructed and anchored to their respective anatomical landmarks. Menisci were placed between the femur and the simplified tibial-fibular platform to simulate joint cushioning and facilitate relative motion (Figure 2b, c). The gastrocnemius muscle was modeled with medial and lateral heads originating from the corresponding femoral condyles (Figure 2d).

A 5-mm-diameter cylindrical rod was used to simulate the Schanz screw or thick pin inserted into the distal femur (Figure 3). Six insertion sites were defined according to standard positions on the distal femoral locking compression plate (LCP) (Depuy Synthes, Oberdorf, Switzerland) and were labeled 1 through 6 (Figure 3a), reflecting typical intraoperative configurations.

Boundary conditions and simulation protocol

The simulation followed a two-stage FEA workflow (Figure 4) to investigate the biomechanical behavior of distal femoral comminuted fracture reduction during intraoperative traction. In Stage I static analysis, a 30 N tensile force was applied to the gastrocnemius muscle to replicate the posterior-inferior displacement and rotational malalignment of the distal femoral fragment. In Stage II static analysis, a 15 N horizontal traction force was applied through the Schanz screw to simulate surgical reduction. The tibial/fibula base and femoral shaft were constrained to replicate intraoperative stabilization. In the model, rotational degrees of freedom were preserved at the screw-bone interface to allow physiologic fragment movement.

This comprehensive simulation framework enabled detailed present of the Quasi-static mechanical interactions among muscle traction, screw-based reduction forces, and bony fragment motion. Reduction outcomes were assessed by

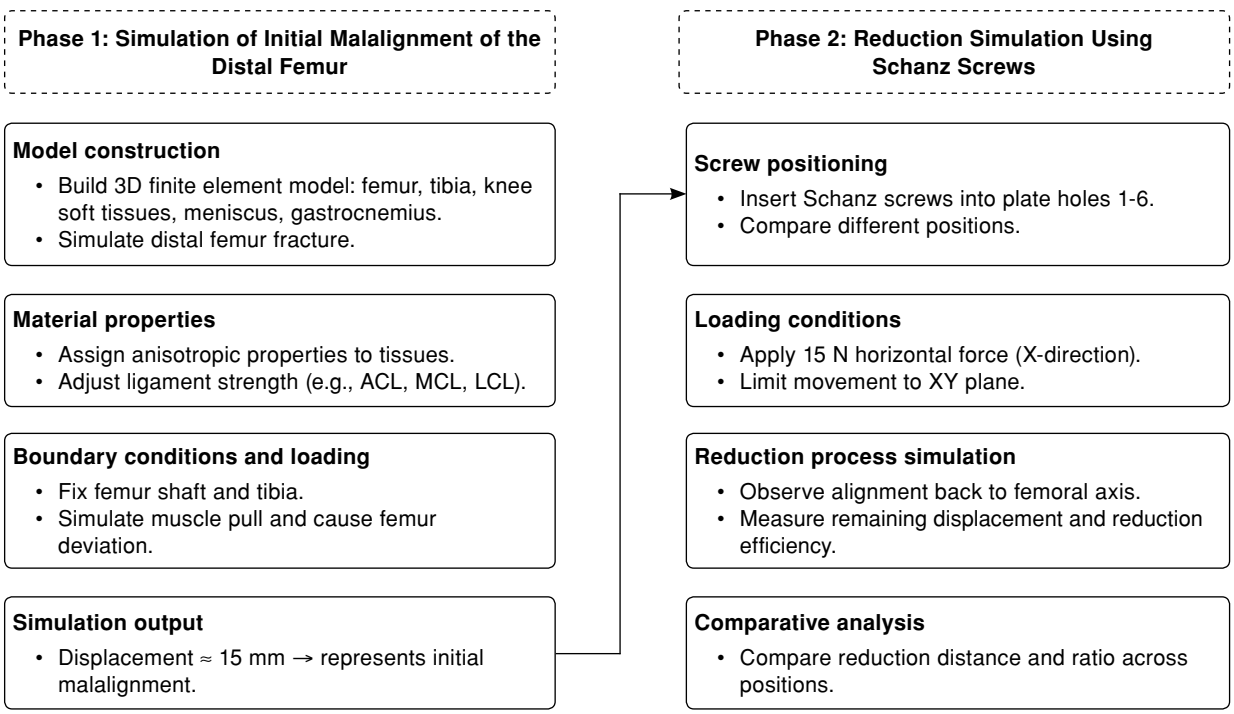


FIGURE 4. Schematic workflow of the two-stage simulation process: initial bone displacement and subsequent reduction via Schanz screw traction.
ACL: Anterior cruciate ligament; MCL: Medial collateral ligament; LCL: Lateral collateral ligament.

TABLE I
Material property settings

Components	Young's Modulus (MPa)	Poisson's ratio
Cortical bone	17,000	0.3
Cancellous bone	1,000	0.3
Tibia plateau	17,000	0.3
Meniscus	59	0.49
Medial collateral ligament	x: 366, y: 1, z: 1	0.4
Lateral collateral ligament	x: 366, y: 1, z: 1	0.4
Anterior cruciate ligament	1	0.4
Posterior cruciate ligament	131.5	0.4
Gastronecmius	1,200	0.3
Scanz screw	200,000	0.3

measuring the residual displacement and angular deviation of the distal fragment following traction at each screw site, enabling quantitative comparison of reduction efficiency.

Material properties and meshing

Material properties were assigned based on values reported in the literature (Table I). The femur was modeled as a two-layer structure comprising cortical and cancellous bone, with Young's modulus (E) set to 17,000 MPa for cortical bone and 1,000 MPa for cancellous bone.[13] A Poisson's ratio of 0.3 was applied uniformly. The Schanz screw, modeled as stainless steel, was assigned a Young's modulus of 200 GPa.[13] For the soft tissues, including the four principal ligaments the MCLs and LCLs, and the ACLs and PCLs (ACL and PCL), as well as the meniscus, properties were set according to literature values.[14-16] Considering the biomechanical behavior of ligaments, which predominantly resist tensile rather than compressive forces, the Young's modulus for the ACL and the MCL/LCL was reduced to 1 MPa to simulate a relaxed, non-load-bearing condition during the early phase of reduction.

For the MCL and LCL, the X-direction (traction direction) stiffness remained as reported in literature to reflect their load-bearing function during Schanz screw traction. However, the stiffness in the Y and Z directions was reduced to 1 MPa to simulate their mechanical slackness in off-axis directions. The PCL, which remains engaged and under tensile load during reduction, was modeled with its original Young's modulus of 131.5 MPa and a Poisson's ratio of 0.4. The gastrocnemius muscle, serving as the source of contractile force in the model, was modeled with an elevated stiffness to ensure force transmission. Without modification, the muscle would primarily deform under load, failing to transmit effective traction to the bone. Therefore, the gastrocnemius was assigned a high stiffness value of 1,200 MPa with a Poisson's ratio of 0.3 to simulate efficient force transmission.[14-16]

The FEA mesh model developed in this study primarily utilized 20-node hexahedral elements as the dominant element type, offering excellent numerical stability and robust capability for nonlinear analyses. In anatomically complex regions, such as curved bone surfaces or ligament attachment sites, 10-node tetrahedral elements were employed to supplement the mesh, thereby enhancing the fidelity of anatomical geometry. For contact interface definitions, the interface between the femur and the Schanz screw was modeled as a nonlinear face-to-face frictional contact with a coefficient of friction of 0.3. Ligament-to-bone attachment sites were assigned bonded conditions, while the meniscus-to-femur contact interface was defined as sliding contact to allow for relative motion and pressure transmission.

The complete mesh configuration and parameters are summarized in Figure 5 and Table II. The cortical bone was assigned a mesh size of 1.80 mm, while cancellous bone and the tibial platform, exhibiting relatively minor geometric variation, were discretized with a coarser mesh size of 5.00 mm. In critical regions with stress concentration such as the bone-screw interface and the meniscus-bone contact zone localized mesh refinement was performed, reducing the minimum

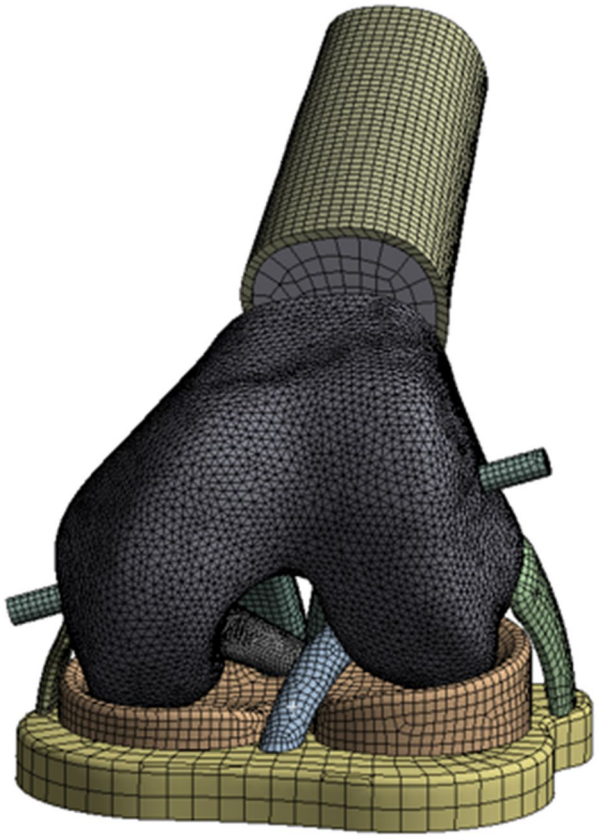


FIGURE 5. Complete mesh configuration of finite element model.

element edge length to 0.5 mm. Other general areas were maintained within a 1.5-2.0 mm range to balance simulation resolution and computational efficiency.

To confirm the suitability of the meshing strategy adopted for the distal femoral reduction model, a mesh convergence analysis

TABLE II
Mesh parameters of finite element model

Components	Element size (mm)
Cortical bone	1.80
Cancellous bone	5.00
Tibia plateau	5.00
Meniscus	2.00
Medial collateral ligament	1.50
Lateral collateral ligament	2.00
Anterior cruciate ligament	1.50
Posterior cruciate ligament	0.75
Gastronecmius	1.50
Scanz screw	1.30

was performed to ensure adequate accuracy without incurring excessive computational cost. Three sets of models with varying average element sizes (coarse, medium, and fine) were compared by evaluating the equivalent stress and displacement at designated monitoring points. The results demonstrated that when the element size was below 1 mm, the distribution of key physical variables stabilized, confirming that the selected mesh settings were sufficient to accurately capture critical biomechanical behaviors during the reduction process.

Overall, the comprehensive FEA model included the femur, tibia, meniscus, major ligaments, and gastrocnemius muscle. The total number of elements ranged between approximately 280,000 and 320,000, with a node count between 850,000 and 950,000, providing a reliable computational framework for simulating the mechanical response of distal femoral fracture reduction.

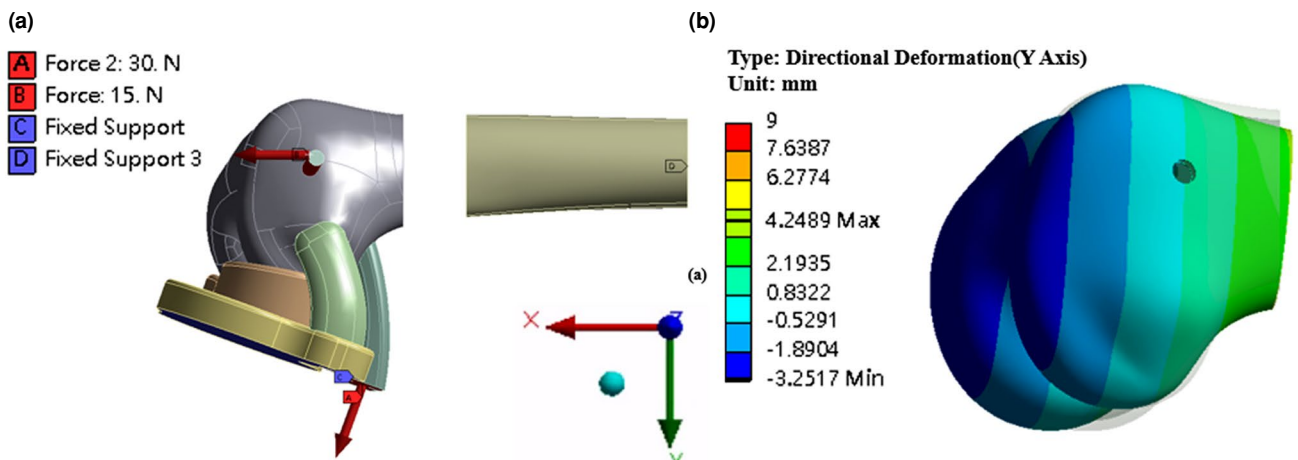


FIGURE 6. Displacement map of the distal femur under simulated gastrocnemius force.

Statistical analysis

Quantitative data obtained from the finite element simulations, including the initial displacement, residual displacement, and reduction ratio of the distal fragment, were analyzed descriptively. The reduction ratio was calculated as the percentage of displacement correction relative to the initial malalignment. Comparative trends across the six Schanz screw positions were assessed numerically to identify the most effective configuration. As this study was based solely on deterministic computational modeling without repeated experimental trials, no formal statistical significance testing was performed.

RESULTS

A 30 N force applied to the gastrocnemius insertion produced a posterior displacement of the distal femoral fragment averaging 14.853 mm, accompanied by a hyperextension deformity (Figure 6). This confirmed that the model effectively captured the characteristic deforming pattern caused by muscle contraction.

When a 15 N horizontal traction force was applied through the Schanz screw to simulate reduction, stress analysis revealed concentrated loading at the screw-bone interface, identifying it as the primary site of force transmission. The effectiveness of reduction varied depending on the

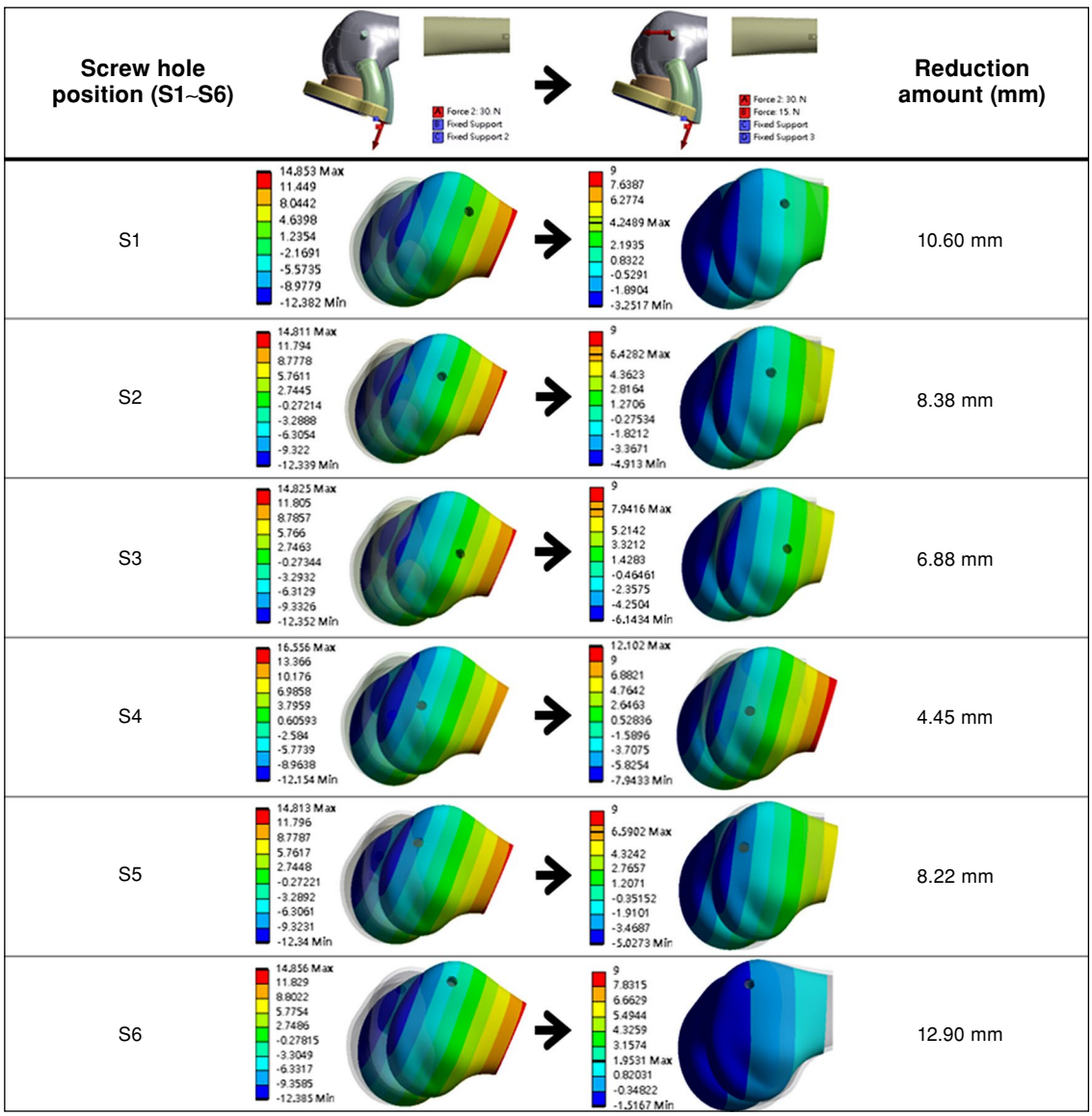


FIGURE 7. Distal femur displacement before and after reduction at various force application positions.

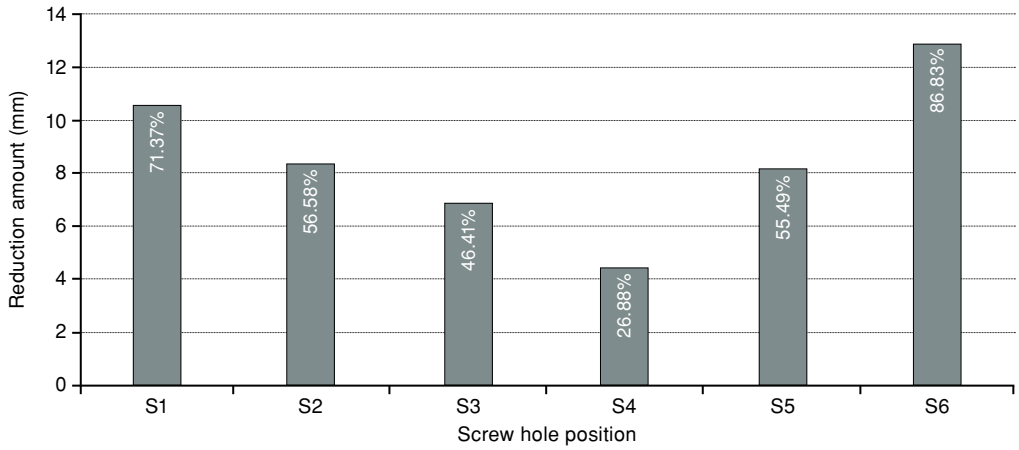


FIGURE 8. Distal femur reduction displacement and ratio across different force application positions.

insertion site of the Schanz screw. Six positions on the distal femoral locking plate were tested, each subjected to the same horizontal traction force. As summarized in Figure 7, initial malalignment distances were comparable across all positions (14.81 to 16.56 mm), but final residual displacements differed substantially, ranging from 1.95 mm (position S6) to 12.10 mm (position S4).

The reduction distances, ranked from greatest to least, were as follows: position S6 (12.90 mm), position S1 (10.60 mm), position S2 (8.38 mm), position S5 (8.22 mm), position S3 (6.88 mm), and position S4 (4.45 mm). The corresponding reduction ratios defined as the percentage of corrected displacement relative to the initial malalignment were as follows: position S6 (86.83%), position S1 (71.37%), position S2 (56.58%), position S5 (55.49%), position S3 (46.41%), and position S4 (26.88%) (Figure 8).

DISCUSSION

The key finding of this study is the identification of the optimal traction site on the distal femur that most effectively corrects supracondylar displacement in distal femoral fractures. This provides a valuable technical reference for surgeons performing fracture reduction. Based on these results, we propose a practical intraoperative approach: the distal femoral plate can be positioned appropriately on the distal fragment, and a long pin inserted through hole position 6 to apply traction. This maneuver effectively counteracts the deforming force of the gastrocnemius muscle. With minimal additional adjustment, the fragment can then be fixed with screws under optimal alignment, thereby simplifying the reduction process.

In distal femur fractures with intra-articular extension, open reduction is typically required to achieve anatomical restoration of the joint surface, followed by stable internal fixation to facilitate primary bone healing. For the extra-articular component, indirect reduction combined with locking plate fixation remains a well-established treatment strategy.[9-11] Critical steps in the indirect reduction process include correcting femoral shortening and addressing hyperextension of the distal fragment, which is primarily caused by contraction of the gastrocnemius muscles.[9] This characteristic deformity pattern was successfully replicated in our FEA model. Under a simulated gastrocnemius traction force of 30 N, the model consistently produced approximately 15 mm of posterior displacement of the distal fragment, closely resembling the deformity observed in clinical scenarios.

A commonly employed intraoperative technique involves applying manual traction to the distal limb while maintaining the knee in flexion, often facilitated by placing a round pillow beneath the knee to counteract the deforming forces exerted by the gastrocnemius.[9] However, in patients with a larger body habitus, sustaining adequate manual traction can be technically challenging, and the force applied may not be efficiently transmitted to the distal fragment. As an alternative, a thick pin, such as a Schanz screw, can be inserted into the distal fragment to allow for direct traction on the distal fragment. This method enables more effective and sustained

force delivery directly to the bone. Based on our clinical experience, this approach is often successful in achieving reduction; however, its effectiveness depends heavily on selecting the optimal pin placement. A detailed analysis of pin placement at various hole positions revealed that more anterior locations provided superior fracture reduction. To illustrate, among holes at the same distal level, hole 1 was more effective than hole 3, and hole 6 outperformed hole 4. This may be attributed to the fact that more anterior pin positions have a longer lever arm relative to the rotational center of the distal femoral fragment. This longer moment arm allows for the generation of greater corrective torque under the same traction force, thereby enhancing the reduction effect. Moreover, the direction of traction at hole 6 is nearly opposite to the pull of the gastrocnemius muscle, effectively neutralizing the deforming force produced by muscle contraction. Overall, pin placement at hole 6 demonstrated the most effective reduction outcome.

In our FEA model, significant differences in fracture reduction performance were observed among the various hole positions. The best-performing hole (hole 6) achieved a reduction ratio of 86.83%, whereas the worst-performing hole (hole 4) yielded only 26.88%. This contrast indicates that selecting an inappropriate hole provides limited benefit for fracture reduction, while choosing the optimal position can effectively counteract the majority of the deforming force. In clinical practice, surgeons may attempt traction through one hole and switch to another if the initial placement proves ineffective. However, using multiple holes may compromise the structural integrity of the bone and reduce the strength of subsequent screw fixation. The findings of this study can assist surgeons in selecting the most suitable hole position from the outset, thereby avoiding less effective attempts and preserving fixation strength. In addition to its biomechanical advantages for fracture reduction, hole 6 is located farther from the supracondylar fracture site, thus minimizing potential disruption to the fracture zone. Furthermore, it is located closer to the subchondral bone, which typically provides denser and stronger bone stock.[17] Applying traction at this location may reduce the risk of secondary bone injury during the procedure.

Nonetheless, this study has several limitations. First, the simulation was based on a standardized experimental femur model and did not account for patient-specific anatomical variations or differences in bone quality. Second, the applied traction force through the Schanz screw was fixed at 15 N along the femoral axis; the study did not investigate the dynamic effects of varying force magnitudes or directions on the reduction process. Third, in real-life surgical settings, additional traction devices and external fixation systems are often employed to assist with reduction. These mechanical contributions were not incorporated into the current model. Nevertheless, the current findings may assist surgeons in identifying the most effective hole position for fracture reduction. In theory, this may help reduce the reliance on additional intraoperative maneuvers or supplementary traction devices. Future studies should investigate varying magnitudes and directions of traction force, as well as the combined effects of multiple reduction devices, to provide a more comprehensive understanding of intraoperative biomechanics. Experimental validation using cadaveric or *in vivo* models is also warranted to confirm the computational findings. Ultimately, incorporating these refinements into clinical trials will be essential for establishing evidence-based guidelines on optimal Schanz screw placement in distal femur fracture reduction.

In conclusion, this FEA study identified hole position 6 on the distal femur as the most effective site for traction-assisted reduction, achieving the greatest correction of deformity. These findings provide objective guidance for pin placement, offering a simple, reproducible strategy to enhance reduction efficiency and surgical outcomes in distal femur fractures.

Data Sharing Statement: The data that support the findings of this study are available from the corresponding author upon reasonable request.

Author Contributions: Were responsible for the study design and conceptualization: S.I.C., T.H.T., S.H.F.; Conducted the study: S.I.C., W.S.H.; Jointly performed the data analysis: S.I.C., W.S.H., T.H.T., S.H.F.; Prepared the manuscript: S.I.C., T.H.T., S.H.F. All authors participated in the revision of the manuscript and responded to the reviewers' comments.

Conflict of Interest: The authors declared no conflicts of interest with respect to the authorship and/or publication of this article.

Funding: This study was supported by the Research Assistantships funded by the National Science and Technology Council, Taiwan (grant number NSTC 113-2221-E-150-001 to Shou-I Chen).

REFERENCES

1. Babhulkar S, Trikha V, Babhulkar S, Gavaskar AS. Current concepts in management of distal femur fractures. Injury 2024;55 Suppl 2:111357. doi: 10.1016/j.injury.2024.111357.

2. Jawad MU, Qubain LM, Kisana HM, Walker JB, Adamczyk AP, McKee MD, et al. Delayed surgical fixation is associated with increased mortality in patients with distal femur fractures. Injury 2025;56:112441. doi: 10.1016/j.injury.2025.112441.
3. Nester M, Borrelli J Jr. Distal femur fractures management and evolution in the last century. Int Orthop 2023;47:2125-35. doi: 10.1007/s00264-023-05782-1.
4. Baris A, Özmen E, Circi E, Yuksel S, Beytemür O. Quantitative analysis of protective Kirschner wire diameters in lateral opening wedge distal femoral osteotomy: A finite element study. Jt Dis Relat Surg 2025;36:97-106. doi: 10.52312/jdrs.2025.1806.
5. Ehlinger M, Ducrot G, Adam P, Bonnomet F. Distal femur fractures. Surgical techniques and a review of the literature. Orthop Traumatol Surg Res 2013;99:353-60. doi: 10.1016/j.otsr.2012.10.014.
6. Wilson JL, Squires M, McHugh M, Ahn J, Perdue A, Hake M. The geriatric distal femur fracture: Nail, plate or both? Eur J Orthop Surg Traumatol 2023;33:1485-93. doi: 10.1007/s00590-022-03337-5.
7. Hake ME, Davis ME, Perdue AM, Goulet JA. Modern implant options for the treatment of distal femur fractures. J Am Acad Orthop Surg 2019;27:e867-75. doi: 10.5435/JAAOS-D-17-00706.
8. Kesemenli C, Subasi M, Necmioglu S, Kapukaya A. Treatment of multifragmentary fractures of the femur by indirect reduction (biological) and plate fixation. Injury 2002;33:691-9. doi: 10.1016/s0020-1383(02)00166-3.
9. Ehlinger M, Adam P, Abane L, Arlettaz Y, Bonnomet F. Minimally-invasive internal fixation of extra-articular distal femur fractures using a locking plate: Tricks of the trade. Orthop Traumatol Surg Res 2011;97:201-5. doi: 10.1016/j.otsr.2010.11.004.
10. Ehlinger M, Adam P, Arlettaz Y, Moor BK, DiMarco A, Brinkert D, et al. Minimally-invasive fixation of distal extra-articular femur fractures with locking plates: Limitations and failures. Orthop Traumatol Surg Res 2011;97:668-74. doi: 10.1016/j.otsr.2011.05.004.
11. Ehlinger M, Scheibling B, Rahme M, Brinkert D, Schenck B, Di Marco A, et al. Minimally invasive surgery with locking plate for periprosthetic femoral fractures: Technical note. Int Orthop 2015;39:1921-6. doi: 10.1007/s00264-015-2928-y.
12. Wu TM, Chien CS, Lin SH. A novel approach to distal femur: A minimally invasive technique for supracondylar and intercondylar fracture. J Orthop Surg Res 2022;17:180. doi: 10.1186/s13018-022-03076-7.
13. Lee CH, Su KC, Chen KH, Pan CC, Wu YC. Impact of tip-apex distance and femoral head lag screw position on treatment outcomes of unstable intertrochanteric fractures using cephalomedullary nails. J Int Med Res 2018;46:2128-40. doi: 10.1177/0300060518775835.
14. Ren D, Liu Y, Zhang X, Song Z, Lu J, Wang P. The evaluation of the role of medial collateral ligament maintaining knee stability by a finite element analysis. J Orthop Surg Res 2017;12:64. doi: 10.1186/s13018-017-0566-3.
15. Wu CH, Liau JJ, Wei HW, Cheng CK. The effect of posterior cruciate ligament deficiency on knee laxity. JCIE 2009;32:53-63.
16. Zhang J, Chen B, Chen B, Wang H, Han Q, Tang X, et al. Clinical application of finite element analysis in meniscus diseases: a comprehensive review. Arch Computat Methods Eng 2025;32:4163-95. doi: 10.1007/s11831-025-10265-0
17. Besa P, Alegría A, González N, Biancardi F, Vidal C, Cikutovic P, et al. Regional bone density patterns of the tibial plateau: Implications for finite element analysis. Front Bioeng Biotechnol 2025;13:1541536. doi: 10.3389/fbioe.2025.1541536.